BIOCHEMISTRY
including biophysical chemistry & molecular biology

Article

pubs.acs.org/biochemistry

Intrinsic Flexibility of West Nile Virus Protease in Solution Characterized Using Small-Angle X-ray Scattering

Andrea P. Garces and Stanley J. Watowich*

Department of Biochemistry and Molecular Biology, University of Texas Medical Branch, Galveston, Texas 77555, United States

ABSTRACT: West Nile virus (WNV) is a mosquito-borne flavivirus with a rapidly expanding global distribution. Infection can cause severe neurological disease and fatality in humans. Efforts are ongoing to develop antiviral drugs that inhibit the WNV protease, a viral enzyme required for polyprotein processing. Unfortunately, little is known about the solution structure of recombinant WNV protease (NS2B-NS3pro) used for antiviral drug discovery and development, although X-ray crystal structures and nuclear magnetic resonance (NMR) studies have provided valuable insights into the interactions between NS2B-NS3pro and peptide-based inhibitors. We completed small-angle X-ray scattering and Fourier transform infrared spectroscopy experiments to determine the solution structure and dynamics of WNV NS2B-NS3pro in the absence of a bound substrate or inhibitor. Importantly, these solution studies suggested that all or most of the NS2B cofactor was highly flexible and formed an ensemble of structures, in contrast to the NS2B tertiary structures observed in crystallographic and NMR studies. The secondary structure of NS2B-NS3pro in solution had high β-content, similar to the secondary structure observed in crystallographic studies. This work provided evidence of the intrinsic flexibility and conformational heterogeneity of the NS2B chain of the WNV protease in the absence of substratelike ligands, which should be considered during antiviral drug discovery and development efforts.

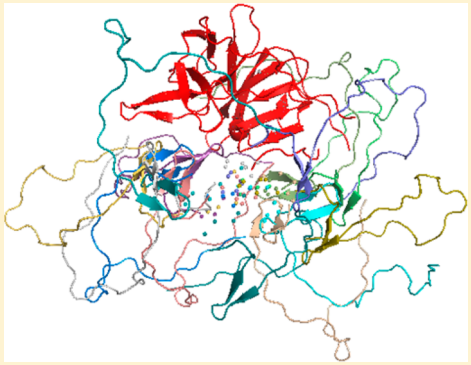

West Nile Virus (WNV) is a single-stranded RNA virus that belongs to the family Flaviviridae.[1] In the past decade, this mosquito-borne virus has been responsible for hundreds of thousands of human infections and tens of thousands of disease cases in the United States.[2] Unfortunately, there are no vaccines or antiviral therapies available to prevent or treat WNV infections in humans.[3]

The WNV genome encodes a polyprotein that includes three structural (C, preM, and E) and seven nonstructural (NS1, NS2A, NS2B, NS3, NS4A, NS4B, and NS5) proteins.[4,5] NS3 has a C-terminal portion that contains a nucleotide/RNA triphosphatase and helicase domain and an N-terminal domain that encodes a serine protease (NS3pro).[3] *In vitro* activity of recombinant NS3pro requires interaction with a hydrophilic segment (~40 amino acids) from transmembrane protein NS2B,[6,7] although the NS3pro activity is only slightly modified by interaction with the C-terminal domain of NS3.[8,9]

The WNV protease is a promising target for antiviral drugs because of its critical role in cleaving the NS2A/B, NS2B/3, NS3/4A, and NS4B/A junctions of the viral polyprotein during post-translational processing.[5,6] Drug discovery studies directed against the WNV protease have traditionally used a recombinant construct that connects a hydrophilic region of NS2B to NS3pro through a Gly-Ser linker; this fused protein has successfully identified peptidic leads such as di- and tripeptide aldehydes, tetrapeptide aldehydes, and D-arginine-based protease inhibitors.[10−13] In addition, low-molecular weight nonpeptidic protease inhibitors have been generated from biochemical high-throughput and structure-based computational screens.[14−17] Small molecule protease inhibitors have exhibited low micromolar kinetic inhibition constants (K_i) with NS2B-NS3pro but have yet to achieve low-nanomolar binding.

To rationally design more potent protease inhibitors, the WNV NS2B-NS3pro linked construct has been crystallized in the absence of substrate[18] and cocrystallized with substratelike peptide (e.g., Naph-KKR-H)[19] and protein (BPTI)[18] inhibitors. In these structures, the C-terminal portion (residues 66−88) of the NS2B chain was observed to adopt significantly different orientations in the absence (termed the "open" structure) and presence (termed the "closed" structure) of inhibitors. In the open structure, the NS2B cofactor and NS3pro active site were separated by ~38 Å (measured from the Cα atom of Asn84 of NS2B to the Cα atom of Ala51 of NS3pro), whereas in the closed structure, the NS2B was wrapped around NS3pro and interacted with inhibitors bound within the active site.

Complementary nuclear magnetic resonance (NMR) studies have been performed to understand inhibitor-induced NS2B conformational changes.[20,21] These solution state studies concluded that both the unbound and inhibitor-bound forms of NS2B-NS3pro existed predominantly as a closed structure in equilibrium with small populations or ensembles of open structures, with the C-terminal region of NS2B (residues 72−90) flexible in the ensembles. Inhibitor binding was suggested to shift the equilibrium to favor even more strongly a closed

Received: June 18, 2013
Revised: September 9, 2013
Published: September 9, 2013

ensemble relative to an open ensemble. Both X-ray and NMR experiments concluded that the dominant structure of WNV NS2B-NS3pro bound to an inhibitor was the closed structure. However, X-ray crystallographic studies suggested the dominant structure of unbound WNV NS2B-NS3pro was the open structure, while NMR studies concluded it was a closed structure.

Much of the ambiguity regarding the unbound NS2B-NS3pro structure centers on the conformation and flexibility of the NS2B chain and the interactions it might make with NS3pro.[18−21] Our current study couples advances in small-angle X-ray scattering (SAXS) with Fourier transfer infrared spectroscopy (FTIR) to determine the likely conformation and structural ensemble of NS2B-NS3pro in the absence of bound substrate or inhibitor. Our results suggest that the NS3pro domain adopts a well-folded compact tertiary structure similar to the observed crystallographic structures. However, the NS2B cofactor appears to adopt multiple conformations distinct from previously described open and closed structures; these conformations could maintain the secondary structure elements observed in crystallographic structures. This detailed structural description of unbound NS2B-NS3pro could aid structure-guided discovery and optimization of WNV protease inhibitors by providing a redefined target in which conformational heterogeneity is incorporated.

MATERIALS AND METHODS

Overexpression and Purification of Recombinant WNV NS2B-NS3pro. A gene fragment encoding WNV NS2B-NS3pro (formed from in-frame concatenation of NS2B residues 48−93, a Gly_4-Ser-Gly_3 linker, NS3 residues 1−188, and a hexahistidine purification sequence; identical to the amino acid sequence of protein structure 3E9019 in the Protein Data Bank) was codon-optimized for *Escherichia coli* expression and commercially synthesized (DNA2.0). The resulting gene was subcloned into expression plasmid pJexpress414 (DNA2.0) and used to transform BL21(DE3) Codon Plus-RIPL *E. coli* cells. Cultures were grown in 2×YT medium (50 mg/mL carbenicillin) at 37 °C until the OD_{600} reached ∼0.6. We induced gene expression by adding 0.5 mM IPTG (isopropyl thio-β-D-1-thiogalactopyranoside) and shaking the sample for 4 h at 37 °C. The cell pellet was resuspended in ice-cold lysis buffer [50 mM HEPES-HCl (pH 7.5), 300 mM NaCl, 10 mM imidazole, 5% glycerol, 300 μg/mL lysozyme, 30 μg/mL DNase, 10 mM $MgCl_2$, and 0.05% Triton X-100] and the clarified supernatant incubated with nickel resin (GE Healthcare) for 1 h at 4 °C. The resin was sequentially washed with 10 and 50 mM imidazole, and bound protein eluted with 500 mM imidazole. Elution fractions containing NS2B-NS3pro were dialyzed at 4 °C against 20 mM glycine-NaOH (pH 9.5) and 5% glycerol. Protein was concentrated and frozen at −80 °C. The final purification utilized size exclusion chromatography with an S75 column (GE Healthcare Life Science) and SAXS buffer [10 mM potassium phosphate (pH 8.0)]. Fractions corresponding to WNV NS2B-NS3pro were collected and concentrated.

Sedimentation Velocity. Experiments were performed with a Beckman-Coulter XL-A centrifuge using 400 μL of protein sample at final concentrations of 0.3 and 2.5 mg/mL in SAXS buffer. Data acquired from runs at 147400*g* and 20 °C were analyzed with SEDFIT22 to generate $c(S)$ versus S plots, where $c(S)$ is the concentration of protein divided by the sedimentation coefficient at the respective S position.[22] The confidence level was set to $P = 0.95$. Theoretical sedimentation coefficients for crystallographic structures were calculated with HYDROPOD (version 10).[23] Theoretical frictional ratios (f/f_0) were obtained using the equations

$$S_{20,w} = M(1 - \nu_{20}\rho_{20,w})/Nf$$

and

$$f_0 = 6\pi\eta(3M\nu/4\pi N)^{1/3} \text{ (Stokes equation)}$$

where M is the molecular weight, ν_{20} is the solute partial specific volume at 20 °C, $\rho_{20,w}$ is the solution density at 20 °C, N corresponds to Avogadro's number, f is the frictional coefficient, f_0 is the minimal frictional coefficient, and η is the solvent viscosity.

Protease Kinetic Assays. Protease activity experiments were performed following previously established protocols.[24] Briefly, purified WNV NS2B-NS3pro and a 7-amino-4-methylcoumarin (AMC)-linked peptide substrate [Boc-GKR-AMC (Bachem)] were incubated at 25 °C in buffers composed of either 10 mM potassium phosphate (pH 8.0) or 50 mM glycine-NaOH (pH 9.5), 30% glycerol, and 1 mM CHAPS. Release of fluorescent AMC was monitored at 10 min intervals for emission at 465 nm (λ_{ex} = 380 nm) using a spectrofluorometer (Fluorolog FL3-22, HORIBA Jobin Yvon). The final protein concentration was 100 nM, while substrate concentrations ranged from 37.5 to 1200 μM. Data were analyzed using Dynafit[25] to determine reaction mechanisms and kinetic parameters.

SAXS Data Collection and Quality Determination. Data were collected using a Rigaku (USA) BioSAXS-1000 Kratky camera on a Rigaku FRE+ X-ray source (Cu target, λ = 1.54 Å) (Table 1). Experiments were performed at 20 °C. Protein samples were filtered through a 100 kDa filter and dialyzed overnight at 4 °C against 10 mM potassium phosphate (pH 8.0). Three different protein concentrations (1.0, 2.5, and 5.6 mg/mL)

Table 1. Data Collection and Scattering-Derived Parameters

Data Collection	
instrument	BioSAXS-1000 (Rigaku)
wavelength (Å)	1.542
q range ($Å^{-1}$)	0.012−0.5
exposure time (min)	60
protein concentration (mg/mL)	2.5
temperature (°C)	20
Structural Parameters	
I_0 (from Guinier)	0.498 ± 0.002
sR_g limits	0.214−1.284
R_g (Å) (from Guinier)	22.7 ± 0.1
R_g (Å) [from $P(r)$]	23.2 ± 0.1
D_{max} (Å)	80 ± 1
R_g (Å), real space/I_0	23.2 ± 0.1/0.5 ± 0.1
R_g (Å), reciprocal space	23.1 ± not determined
Porod volume estimate ($Å^3$)	46000 ± 5000
Software Employed	
primary data processing	SAXSLab
data analysis	PRIMUS (ATSAS, suite 2.3)
generation of theoretical intensities	CRYSOL
ab initio modeling	DAMMIF, DAMAVER, SUPCOMB
modeling of conformational ensembles	ensemble optimization method (EOM)
mixture analysis	OLIGOMER
three-dimensional graphics representations	Pymol

dx.doi.org/10.1021/bi400782w | *Biochemistry* 2013, 52, 6856−6865

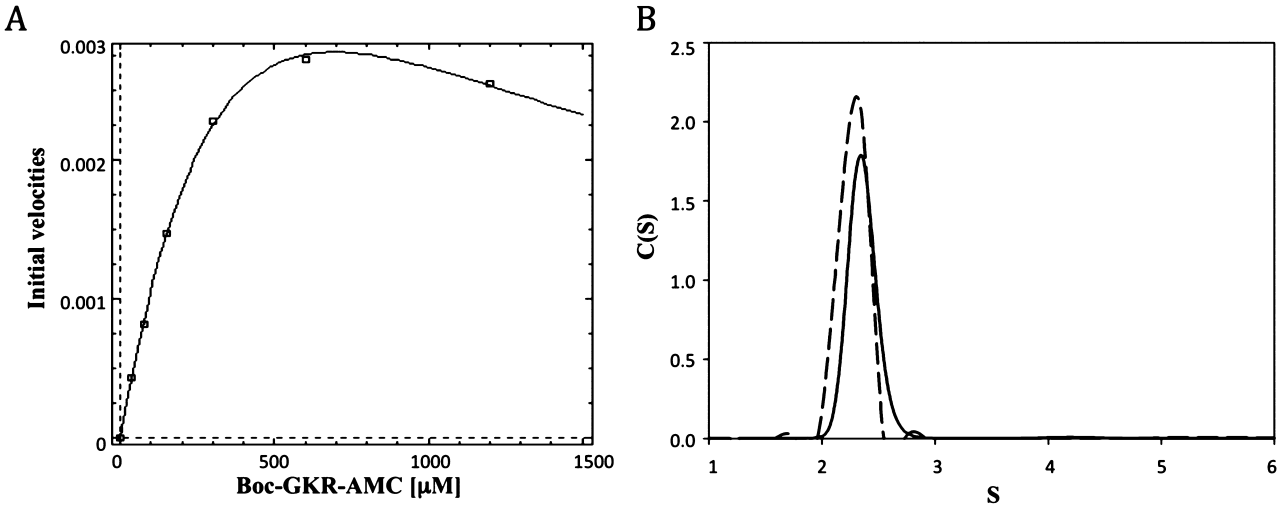

Figure 1. Test for the functionality and oligomerization state of WNV protease. (A) Saturation curve showing WNV NS2B-NS3pro activity with a Boc-GKR-AMC peptide substrate in 10 mM potassium phosphate (pH 8.0). The substrate inhibition model (—) (K_d = 585 ± 67 μM, K_{d2} = 827 ± 120 μM, and k_{cat} = 0.074 ± 0.006 s^{-1}) provided the best fit to the experimental data points (□). (B) Sedimentation velocity experiment with 2.5 mg/mL (– – –) and 0.3 mg/mL (—) WNV protease in 10 mM potassium phosphate (pH 8.0). The absorbance was measured at 298 nm (2.5 mg/mL sample) and 280 nm (0.3 mg/mL sample).

were examined for aggregates and/or electrostatic repulsion in the sample. SAXS data were collected from averaging three to six experiments, each with a 60 min exposure. No radiation damage was detected after samples had been exposed for 60 min during a 10 h experiment at 20 °C (data not shown). Buffer absorbance spectra were separately recorded and subtracted from sample spectra prior to data processing.

Data processing was conducted with SAXSLab (Rigaku) (Table 1), and data analysis was performed using PRIMUS (suite 2.3, ATSAS).[26] Determination of SAXS data quality and folding states was based on analysis of the Guinier region and Kratky plots, respectively.[26] The scattering intensity at zero angle (I_0) and the radius of gyration (R_g) were evaluated using the Guinier approximation: $\ln(I) \sim \ln(I_0) - {}^1/_3(qR_g)^2$, with the limit $qR_g < 1.3$.[27] In addition, R_g and the maximal distance in the particle (D_{max}) were determined from pair distance distribution function $P(r)$, which was obtained by indirect Fourier inversion of the entire scattering curve using GNOM.[27,28] The hydrated volume was obtained from the Porod invariant, and the molecular weight was computed by scaling the Porod volume by 0.59.[27,28]

SAXS Data Analysis. Theoretical scattering curves were generated using the CRYSOL software package.[29] Crystallographic structures of either the open [Protein Data Bank (PDB) entry 2GGV][18] or the closed (PDB entry 3E90)[19] structures of WNV NS2B-NS3pro were fit to the experimental scattering data. The agreement between theoretical and experimental scattering curves was evaluated by discrepancy value χ^2 within a range of $q < 0.5$.[27]

Ab initio modeling used DAMMIF[30] to complete simulated annealing of single-phase dummy atom models. Twenty independent models were calculated with no symmetry restrictions. DAMAVER[31] was used to align *ab initio* models, select the most likely models, and build averaged models. The mean and standard deviation of the normalized spatial discrepancy (NSD) were calculated as 0.7 and 0.09, respectively, indicating the model reconstructions were reliable. SUPCOMB[30] was used to superimpose crystallographic structures within the averaged molecular envelope.

The ensemble optimization method[32] was used to select conformational ensembles that best represented the experimental SAXS data. This software consisted of two parts: RANCH (RANdom CHain) generated a pool of 10000 random models based upon sequence and structural constraints, and GAJOE (Genetic Algorithm Judging Optimization of Ensembles) used a genetic algorithm to randomly select models from the pool whose theoretical scattering curves best approximated the experimental SAXS data.[32] Six ensemble models (Figure 4A) were constructed to test NS2B chain models with differing degrees of flexibility; in each model, the NS2B chain was linked to a rigid NS3pro structure. Model NS2B-NT assumed residues 51–72 of the NS2B chain were flexible, while the C-terminus of NS2B and the NS3pro domain were rigid with a structure described by the closed structure of NS2B-NS3pro (PDB entry 3E90).[19] Model NS2B-DDD assumed residues 51–83 of the NS2B chain, including the DDD triad, were flexible and the remainder of the molecule was rigid with a structure described by the closed structure of NS2B-NS3pro. Model NS2B-U assumed residues 51–97 of the NS2B chain were flexible and the NS3pro domain was rigid as described by the closed structure of NS2B-NS3pro. Model NS2B-CT represented the C-terminus of NS2B (starting from Glu73) as a random coil and assumed the N-terminus of NS2B maintained the crystallographic secondary structure but was free to reorient because it linked to the flexible C-terminus of NS2B. Model NS2B-F assumed the Gly_4-Ser-Gly_3 linker between the NS2B and NS3pro segments was flexible and the NS2B chain adopted the conformation described by the closed structure of NS2B-NS3pro. In models NS2B-CT and NS2B-F, the positions of the rigid regions of NS2B were highly variable because they were located upstream of the NS2B flexible regions and thus dependent on the position and orientation of the N-terminus of the flexible region. A sixth model was generated to mimic the conformational state suggested by NMR studies;[20] in this model, the C-terminus of NS2B was flexible and the N-terminus of NS2B was constrained to interact with NS3pro (NS2B-CTf). SAXS parameters for the ensemble models were calculated with GNOM and DATPOROD subroutines.[27,28]

dx.doi.org/10.1021/bi400782w | *Biochemistry* 2013, 52, 6856–6865

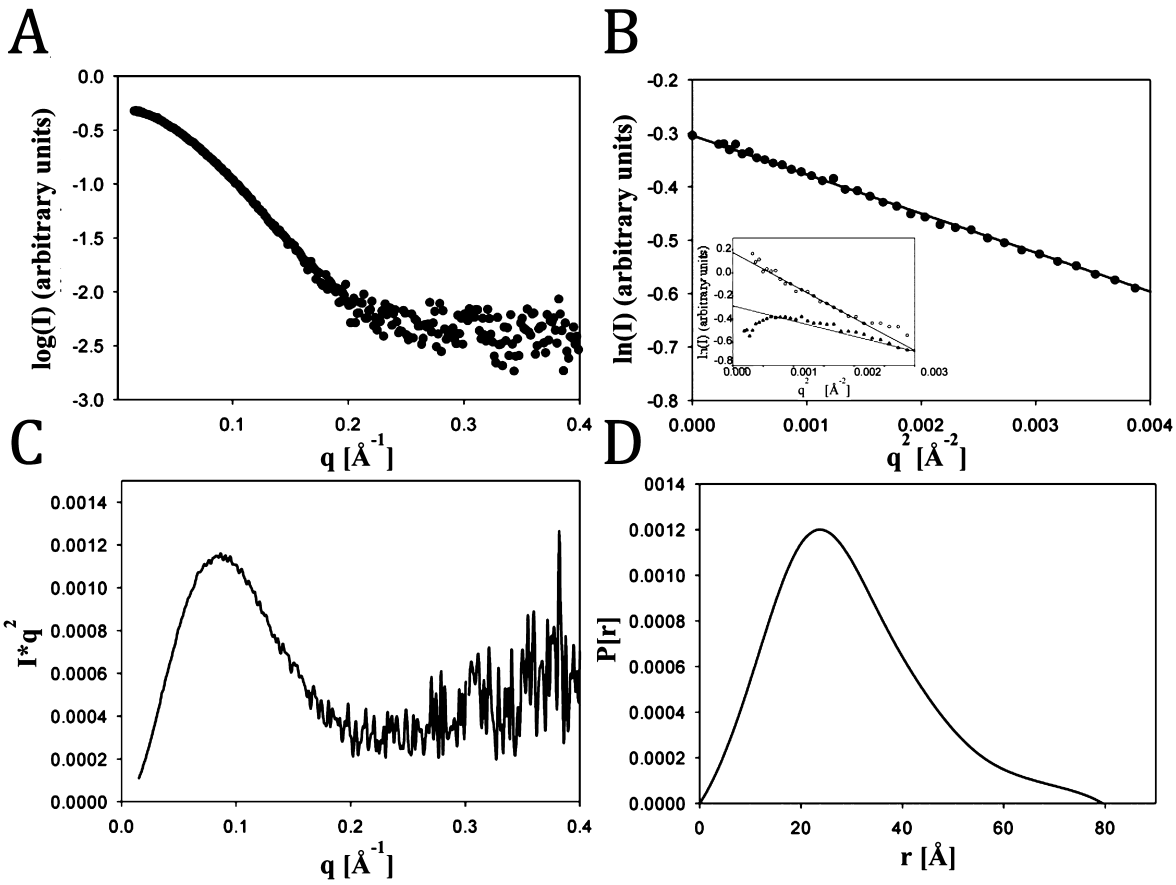

Figure 2. SAXS solution characterization of WNV NS2B-NS3pro. Small-angle X-ray scattering (SAXS) data collected from 2.5 mg/mL WNV protease after overnight dialysis against 10 mM potassium phosphate (pH 8.0). (A) Experimental SAXS data from WNV protease. (B) Guinier plot (processed with PRIMUS). The inset shows a Guiner plot of WNV protease at 1 mg/mL (○) and 5.6 mg/mL (▲). (C) Kratky plot. Scattering pattern as q^2I vs q. (D) Pair distance distribution plot from experimental WNV protease data obtained using GNOM.[26]

OLIGOMER[27] was used to test if mixtures of NS2B-NS3pro structures produced scattering curves consistent with the observed SAXS data. This program could identify the volume fraction of each component in a mixture that best fit the experimental SAXS data.[27] Analysis were performed with crystal structures corresponding to the open (PDB entry 2GGV)[18] and closed (PDB entry 3E90, chain A)[19] structures of NS2B-NS3pro.

Fourier Transform Infrared Spectroscopy (FTIR). Aliquots of purified WNV NS2B-NS3pro in SAXS buffer were lyophilized overnight and resuspended in D_2O. Samples were incubated at 4 °C overnight, filtered through a 100 kDa molecular mass cutoff filter (Millipore), and concentrated. Control experiments were performed and confirmed the lyophilization protocol did not affect protease activity (data not shown). FTIR experiments were conducted using a JASCO FT/IR-4100 spectrometer. Protein samples (20 mL of a 2.5 mg/mL solution) were added to the top of a diamond PRO450-S attenuated total reflectance unit adapted to the FT/IR-4100 system. The protein-containing drop was left in the FTIR-ATR device, and consecutive spectra were recorded at higher protein concentrations (resulting from continued water evaporation) until the variation in residual parameters, which reflected the degree of deviation between the experimental sample and the Jasco protein library database, was minimized. An exact determination of protein concentration was not necessary for secondary structure analysis using Jasco-supplied software.[33] Experimental parameters included 64 scans per protein sample with a 4.0 cm^{-1} resolution. Deuterated buffer spectra were collected and subtracted from protein sample spectra. Data fitting and secondary structure estimations were done by multicomponent analysis through the Secondary Structure Estimation (SSE) software;[33] amino acids present in recombinant NS2B-NS3pro but not in the crystallographic structures (e.g., the hexahistidine sequence) were thought to adopt a random coil.

RESULTS

Purified WNV NS2B-NS3pro Was Functionally Active and Monomeric in Solution. WNV NS2B-NS3pro was overexpressed in *E. coli* and purified as described and according to standard protocols.[34] No self-cleavage of the protein was observed as monitored by Coomassie blue staining of samples separated via sodium dodecyl sulfate−polyacrylamide gel electrophoresis (data not shown). WNV NS2B-NS3pro was tested for protease activity using Boc-GKR-AMC as a substrate[24] and showed catalytic activity in 10 mM potassium phosphate (pH 8.0) (Figure 1A). Substrate inhibition was clearly evident at substrate concentrations of >600 μM (Figure 1A). The following kinetic parameters were calculated: K_d = 585.4 ± 67 μM, K_{d2} = 827 ± 120 μM, and k_{cat} = 0.074 ± 0.006 s^{-1} (they were consistent with kinetic parameters generated in buffers typically used for NS2B-NS3pro inhibition studies).[24]

Sedimentation velocity experiments concluded that purified NS2B-NS3pro was essentially homogeneous in solution with a molecular mass of ~28 kDa for the predominant (>99%) species;

dx.doi.org/10.1021/bi400782w | *Biochemistry* 2013, 52, 6856−6865

Table 2. Values of SAXS Parameters

		theoretical data							
		crystallographic structures[a]		ensemble of conformations[c]					
structural parameter	experimental data	closed state	open state	NS2B-CTf	NS2B-NT	NS2B-DDD	NS2B-U	NS2B-CT	NS2B-F
χ^2	–	4.24	5.04	3.0	2.94	1.80	1.13	1.06	1.06
R_g (Å) (from Guinier)	22.7 ± 0.1	19.8	20.0	20.4	20.7	21.4	22.8	23.0	22.9
R_g (Å) [from $P(r)$]	23.2 ± 0.1								
D_{max} (Å)	80 ± 1	57.5	63.6	70	75	72	80	78	78
Porod volume estimate (Å^3)	46000 ± 5000	33000	32000	43000	42000	44000	44000	48000	47000
molecular mass (kDa)[b]	27.0 ± 2.7	23.9	23.3	25.5	24.6	26.1	25.7	28.1	27.7

[a]Bound structure taken from PDB entry 3E90 (chain A);[19] substrate-free structure taken from PDB entry 2GGV.[18] Data calculated with CRYSOL. [b]Molecular mass determined from the Porod volume, with an error of ~10%. [c]SAXS parameters for ensemble models calculated using GNOM and DATPOROD.

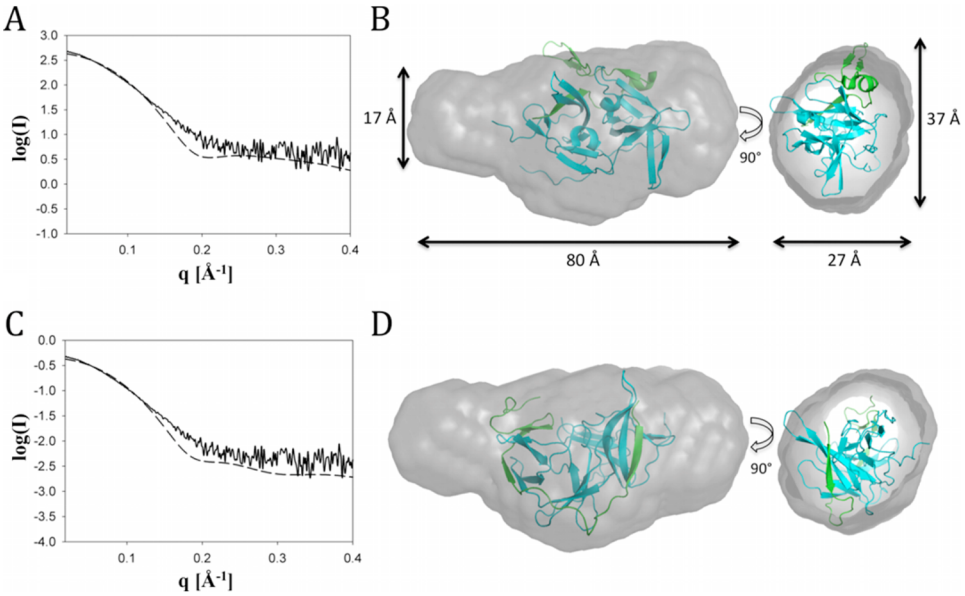

Figure 3. Comparison of SAXS data collected from solutions of WNV NS2B-NS3pro and calculated from NS2B-NS3pro crystallographic structures. (A) Experimental scattering curve from WNV protease in solution (—) and theoretical scattering curve calculated from the open crystal structure (– – –). (B) WNV NS2B-NS3pro in the open structure superimposed on the envelope produced from averaged *ab initio* models that best fit experimental SAXS data of WNV protease. (C) Experimental scattering curve from WNV protease in solution (—) and theoretical scattering curve calculated from the closed crystallographic structure (– – –). (D) WNV closed structure superimposed on the envelope produced from averaged *ab initio* models that best fit experimental SAXS data of WNV protease.

this molecular mass was consistent with the molecular mass expected for a monomer of WNV NS2B-NS3pro. Similar results were observed when NS2B-NS3pro was analyzed at concentrations of 0.3 and 2.5 mg/mL, suggesting the monomeric state was independent of protein concentration (Figure 1B). The frictional ratio of WNV NS2B-NS3pro calculated from sedimentation velocity experiments was 1.44, which was higher than the ratio of 1.2 typically observed for globular spherical proteins.[35] Theoretical frictional ratios for NS2B-NS3pro in closed (PDB entry E390) and open (PDB entry 2GGV) structures were calculated as 1.23 and 1.28, respectively. These solution state characterization studies suggested that WNV NS2B-NS3 protease was active and monomeric and did not completely adopt the compact globular state described by X-ray crystallographic studies.[18,19]

The NS2B-NS3pro Solution State Conformation Differed from Reported Crystallographic Structures. SAXS experiments were performed to determine the structure of WNV NS2B-NS3pro in solution. No radiation damage was detected during data collection at 20 °C (data not shown), and data collected for 60 min from solutions of 2.5 mg/mL NS2B-NS3pro generated reproducible scattering curves for q values of >0.2 (Figure 2A). The linearity of Guinier plots at $qR_g < 1.3$ ($r = 0.98$) (Figure 2B) was an indication of good data quality, with no evidence of aggregation or interparticle repulsion.[27] Interparticle repulsion was observed at 5.6 mg/mL protein with a predicted R_g value of ~20 Å, whereas the sample with 1 mg/mL protein did not produce good quality data and indicated an R_g of ~29 Å (Figure 2B, inset). Kratky plots (Iq^2 vs q)[26] of SAXS data have been used to estimate the folding state of proteins in solution; compact globular proteins exhibited defined peaks in Kratky plots, while conformationally disordered or elongated proteins showed a tendency for increased Iq^2 values at high q values.[27] The Kratky plot of WNV NS2B-NS3pro showed a local maximum at $q \sim 0.1$ Å, and this curve did not return to baseline at $q \sim 0.2$ Å (Figure 2C). In addition, the Iq^2 value trended upward at q values of greater than ~0.2.

dx.doi.org/10.1021/bi400782w | *Biochemistry* 2013, 52, 6856–6865

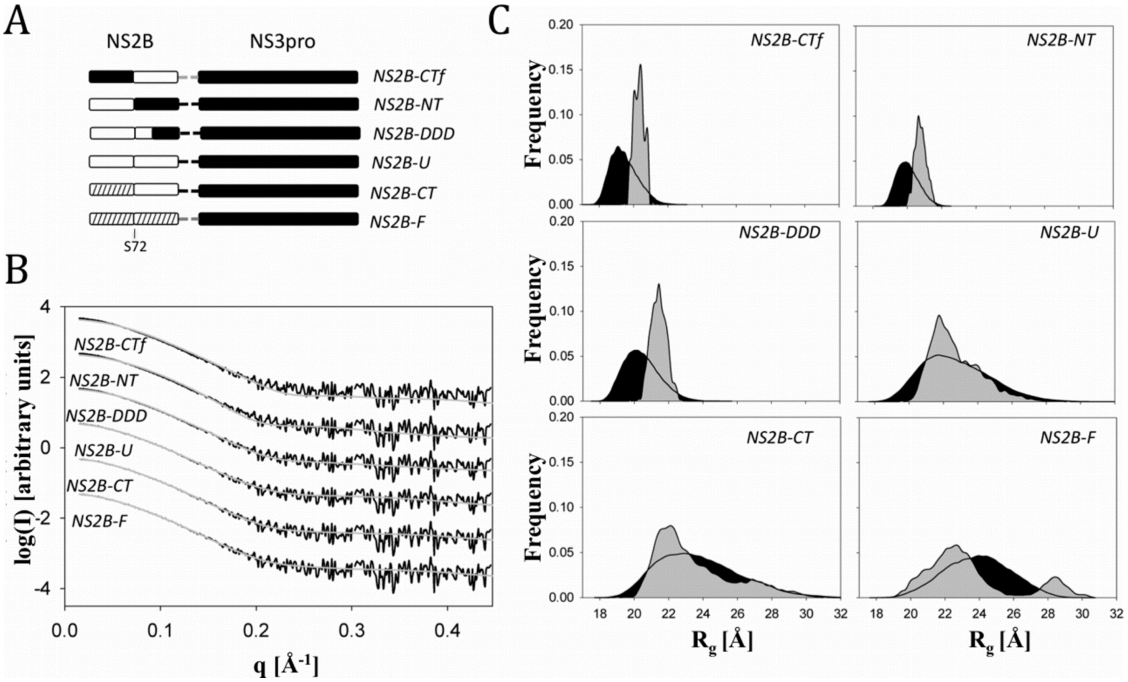

Figure 4. Ensemble optimization method. Six different ensemble models of NS2B flexibility were constructed and compared with experimental SAXS data from substrate-free WNV NS2B-NS3pro. (A) Graphical representation of models NS2B-CTf, NS2B-NT, NS2B-DDD, NS2B-U, NS2B-CT, and NS2B-F. Regions modeled as in the crystal structure are colored black; flexible regions are colored white, and rigid but mobile regions are indicated with hashed lines. (B) Fitting curves of the theoretical scattering models (gray dashed solid lines) and experimental SAXS data (black solid line). (C) Distribution of the radius of gyration (R_g) of random (black) and selected (gray) pools for all the models. Ensembles selected for models NS2B-CTf, NS2B-NT, NS2B-DDD, and NS2B-U had average R_g values of 20.4, 20.7, 21.4, and 22.9 Å, respectively. Ensembles selected for models NS2B-CT and NS2B-F had bimodal R_g distributions with peaks around 22 and 28 Å.

An alternative method for characterizing the shape of a particle in solution is a pair distance distribution [$P(r)$] plot, which represents distances between all electrons within a macromolecule.[26,27] The asymmetrical shape and "tail" of $P(r)$ with large radii (Figure 2D) suggested that WNV NS2B-NS3pro was not folded into a compact globular structure. The radii of gyration (R_g) for WNV NS2B-NS3pro were 22.7 ± 0.1 and 23.2 ± 0.1 Å (Table 2) as calculated from Guinier plots and pair distance distribution functions [$P(r)$],[27] respectively. In addition, $P(r)$ plots suggested the maximal distance (D_{max}) of WNV NS2B-NS3pro was 80 ± 1 Å (Figure 2D). These results were consistent with the hypothesis that in solution WNV NS2B-NS3pro was partially folded with highly flexible regions.

SAXS data provided no evidence of NS2B-NS3pro oligomerization, in agreement with conclusions from sedimentation velocity studies. The apparent molecular mass of WNV NS2B-NS3pro in solution was estimated by its hydrodynamic volume using the Porod approximation;[27] these calculations yielded a Porod volume of 46000 ± 5000 Å^3 and an apparent molecular mass of 27 ± 3 kDa (Table 1). The apparent molecular mass calculated from the Porod volume was consistent with the molecular mass of 26.6 kDa calculated from the amino acid sequence of monomeric WNV NS2B-NS3pro.

Theoretical scattering curves were generated and compared to the experimental solution scattering data to determine if the solution conformation of WNV NS2B-NS3pro was represented by the open (PDB entry 2GGV) or closed (PDB entry 3E90) NS2B-NS3pro crystal structures.[18,19] Agreement between theoretical and experimental curves was quantitatively evaluated using χ^2 values, where a χ^2 of 1 indicated an exact fit between the curves and higher values represented increasingly poorer fits between the model and experimental data.[29] Theoretical scattering curves for the open and closed structures did not fit the experimental SAXS data (Figure 3A,C) and had χ^2 values of 5.04 and 4.24, respectively (Table 2). These results suggested that the individual open and closed X-ray structures were not good representations of the WNV NS2B-NS3pro structure in solution.

We next examined if the solution state might contain an equilibrium mixture of open and closed structures, as suggested by NMR studies.[20,21] Calculations with OLIGOMER[27] produced scattering curves with a χ^2 value of 5.47 (data not shown), suggesting that the presence of only these two crystallographic structures in equilibrium did not provide a good model for the experimental data.

Structural parameters extrapolated from the modeled and experimental scattering data were compared to further determine if available crystallographic structures might be consistent with the experimental data (Table 2). The open and closed structures had similar R_g values of 19.8 and 20.0 Å, respectively. In contrast, the open and closed structures had different D_{max} values of 63.6 and 57.5 Å, respectively. Importantly, the R_g and D_{max} parameters for the crystallographic structures were significantly smaller than the values obtained from experimental SAXS data for WNV protease in solution (Table 2).

The shape and compactness of WNV NS2B-NS3pro in solution could be approximated with *ab initio* models that produced small-angle X-ray scattering curves that matched the experimental curves. Using DAMMIF,[30] 20 independent models were produced with no symmetry restrictions. The mean value of the normalized spatial discrepancy (NSD) was 0.7 ± 0.1, indicating a high degree of similarity between all models. The χ^2 between scattering curves generated from selected reference models and the experimental scattering data was 1.12, which

indicated the *ab initio* models were reasonable representations of the solution state structure. The averaged envelope for the *ab initio* models exhibited a roughly elongated ovoid shape with approximate dimensions of 27 Å × 37 Å × 80 Å (Figure 3B,D); the longest dimension was similar to the D_{max} determined from the pair distance distribution plot. Superimposition of NS2B-NS3pro crystallographic structures and the *ab initio* envelope produced NSD values of 2.28 and 2.24 for the open and closed structures, respectively. These results provided further evidence that WNV NS2B-NS3pro X-ray structures were not representative of the protease's folded state in solution.

Solution State Models with a Flexible NS2B Cofactor Were Consistent with the Experimental SAXS Data. Because the crystallographic structures of WNV protease were unable to provide reasonable models for the WNV protease solution state, ensemble models with varying degrees of NS2B flexibility and movement (Figure 4A) were constructed with the ensemble optimization method.[32] Theoretical SAXS curves were calculated for each ensemble model and compared to the experimental scattering data (Figure 4B and Table 2). Among the tested ensemble models, NS2B-CTf and NS2B-NT showed the poorest agreement between calculated and experimental scattering curves with χ^2 values of 3.0 and 2.94, respectively. The scattering curve for the NS2B-DDD ensemble model also had poor agreement [χ^2 = 1.80 (Table 2)] with the experimental data. These results suggested that the solution state of WNV protease could not be represented as an ensemble of conformations if the conformations retained a significant portion of the NS2B crystallographic structure. The calculations described above used the closed crystallographic structure to model the rigid regions of the ensembles; similar χ^2 values (and conclusions) were obtained when the open crystallographic structure was used to model the rigid regions of the ensembles.

The NS2B-U ensemble model, which assumed the entire NS2B chain was unfolded and flexible, produced a scattering curve in very good agreement [χ^2 = 1.13 (Table 2)] with the experimental data. NS2B-CT and NS2B-F were equally plausible ensemble models for the solution state of WNV protease, as judged by χ^2 values [χ^2 = 1.06 (Table 2)]. These models combined flexible NS2B C-terminal regions with rigid NS2B N-terminal regions constrained to the conformation observed in the crystallographic structures. In these ensemble models, the NS2B chain, although conformationally rigid, was mobile and occupied highly variable spatial positions because it was attached to the flexible linker.

The relative distribution of the radius of gyration (R_g) for randomly generated structures and the best-fit ensemble structures from the models described above provided a powerful method for characterizing the solution state of WNV protease. The set of randomly generated structures for each model followed a normal R_g distribution that ranged from very compact (R_g < 19 Å) to very extended structures (Figure 4C). The complete set of structures for the NS2B-NT ensemble model had R_g distributions that ranged from ∼18 to ∼22 Å, whereas the best-fit ensemble structures for NS2B-NT displayed a narrow R_g distribution with an average value of 20.7 Å. The NS2B-CTf ensemble model exhibited an average R_g value of 20.4 Å. (Figure 4C and Table 2). In contrast, the best-fit ensemble structures of NS2B-DDD had an average R_g of 21.4 Å (Figure 4C and Table 2). The best-fit ensemble structures for NS2B-U, NS2B-CT, and NS2B-F had a comparable average R_g of ∼22.9 Å (Table 2); these values were similar to the R_g calculated from Guinier and pair distance distribution plots for WNV protease (Table 2). In addition, the best-fit ensemble models for NS2B-CT and NS2B-F had a bimodal R_g distribution with peaks observed at R_g values of ∼22 and ∼28 Å (Figure 4C). This observation suggested that two subensembles might be present in solution, with the flexible NS2B region adopting different conformational states in each ensemble. The more compact conformation represented ∼85% of the population, while the extended conformation represented ∼15% of the conformational population in NS2B-CT and NS2B-F ensemble models.

Protease models in which the entire NS2B cofactor was mobile and not bound to the NS3pro domain most closely reproduced the SAXS experimental data. Interestingly, the theoretical scattering curves (and χ^2 values) were similar for ensemble models in which the NS2B chain was treated as fully flexible (e.g., NS2B-U) or as a rigid conformation attached to a short flexible linker at the C-terminus of NS2B (e.g., NS2B-CT and NS2B-F). The major requirement for reproducing the SAXS data was the ability of the entire NS2B chain to sample numerous conformations, including a significant number of highly extended conformations. A detailed examination of the members of the NS2B-F ensemble model (Figure 5) did not identify individual conformations that adopted NS2B orientations similar to those observed in the open or closed crystallographic structures.

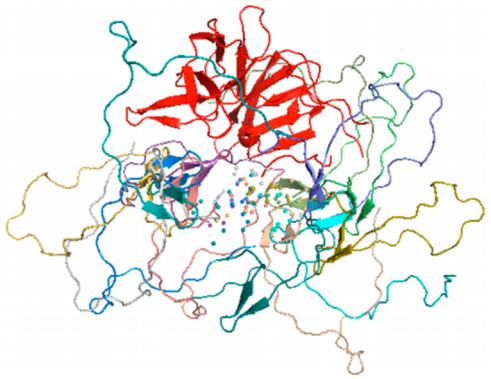

Figure 5. Ensembles of selected conformations of model NS2B-F. NS3pro is colored yellow, while the NS2B cofactor is shown in different orientations, each of which retained the crystallographic secondary structure elements. The flexible linker is represented with spheres. This figure was generated with Pymol.

FTIR Studies Suggested NS2B-NS3pro Developed Similar Secondary Structure in Solution and in Crystalline Environments. The extent of secondary structure predicted for the NS2B cofactor was a major structural difference among the NS2B-U, NS2B-CT, and NS2B-F ensemble models that best fit the SAXS data. FTIR experiments were performed to determine the secondary structure content of WNV NS2B-NS3pro in solution. This technique has been widely used to estimate secondary structure content in proteins.[36−41]

Spectra corresponding to the amide I band were collected and deconvoluted into Gaussian components that described principal secondary structure elements using a matrix method (Figure 6).[40] This analysis suggested that WNV protease in solution was approximately 3% α-helix, 68% β-strand and β-turn, and 29% nonregular secondary structure (random or non-α/non-β conformation) (Table 3). The FTIR secondary structure content was compared with secondary structure elements present in the open and closed crystallographic structures and the ensemble models (Table 3). The NS2B chain in the open and closed crystallographic structures contained a β-hairpin turn toward the

dx.doi.org/10.1021/bi400782w | *Biochemistry* 2013, 52, 6856−6865

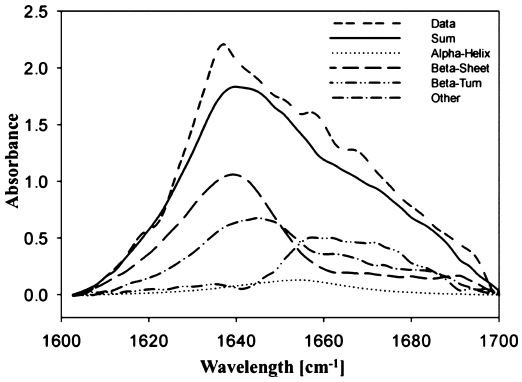

Figure 6. WNV NS2B-NS3pro secondary structure determined by FTIR. Spectral deconvolution of the FTIR amide I band of WNV NS2B-NS3pro.

Table 3. Comparison of Secondary Structure Contents Determined by FTIR and Calculated from Model Structures

	α content (%)	β content (%)[b]	other (%)
experimental FTIR data[a]	3	68	29
closed structure (PDB entry E390)	2	51	47
open structure (PDB entry 2GGV)	6	50	44
model NS2B-CTf	2	45	53
model NS2B-NT	2	46	52
model NS2B-DDD	2	43	55
model NS2B-U	2	40	58
model NS2B-CT	2	45	53
model NS2B-F	2	51	47

[a]Average of 10 measurements, each of 64 scans. [b]Sum of β-turn and β-sheet content.

C-terminus (residues 78−86) and two β-strands a total of ∼16 residues in length. These elements were used to calculate the secondary structure content of the different ensemble models. The FTIR results (Table 3) were most consistent with an NS2B chain that contained significant secondary structure, confirming the high content of β-elements present in the folding state of WNV protease in solution. Although the identification of just one EOM model as the best representative of the WNV protease conformation was difficult, it was clear that extensive conformational heterogeneity was present with the NS2B chain.

The NS2B chain in model NS2B-F retained significant β-strand and β-turn secondary structural elements. Moreover, this model assumed the linker between the NS2B and NS3pro chains was flexible, which allowed even a rigid NS2B chain to sample multiple spatial configurations and explore different orientations with respect to NS3pro. Transient interactions between the NS2B chain and the NS3pro domain could occur, and these interactions may stabilize the distinct subpopulations observed in the structures that comprise the NS2B-F ensemble model and/or preserve the secondary structure suggested by FTIR (Figure 5).

DISCUSSION

West Nile virus NS2B-NS3pro is a promising antiviral target because it plays a critical role in processing the viral polyprotein by cleaving specific junctions to regulate viral nonstructural protein activities necessary for virus maturation and replication.[1,3] X-ray crystallography and NMR experiments characterized the WNV protease folding state, but there was poor agreement between the NMR and crystallographic structures for the unbound (substrate/inhibitor-free) protease. NMR studies proposed NS2B residues 72−97 were in equilibrium between a predominantly closed structure and a small population of open conformations,[20,21] while X-ray crystallography proposed a compact open structure in which the NS2B cofactor (residues 50−88) was stabilized with a Trp62 "anchor" that allowed the N-terminal region of NS2B to fold around the NS3pro domain (Figure 7).[18] These differences between the crystallographic and

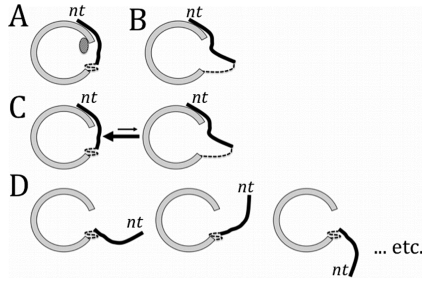

Figure 7. Schematic representation of WNV NS2B-NS3pro structures. (A) Structure of NS2B-NS3pro bound to an inhibitor as determined by X-ray crystallography (i.e., closed structure). (B) Structure of unbound NS2B-NS3pro as determined by X-ray crystallography (i.e., open structure). (C) NMR experiments described the unbound NS2B-NS3pro in equilibrium between the closed structure and a small ensemble of open structures. (D) SAXS experiments (this work) concluded the solution state of unbound NS2B-NS3pro was a conformational ensemble with a flexible NS2B chain bound to a structured NS3pro domain (see Figure 5). The NS2B, Gly-Ser linker, and NS3pro segments are represented as solid black lines, dashed lines, and solid gray lines, respectively. The N-terminus of the NS2B-NS3pro protein is labeled *nt*.

NMR structures of unbound WNV NS2B-NS3pro may stem from the inactivating H51A mutation used to determine the crystallographic open structure or the limited quality HSQC spectra used to determine the NMR structure. Structure-guided design of protease inhibitors may benefit from a detailed understanding of the structure and flexibility of substrate/inhibitor-free WNV NS2B-NS3pro in solution, including the conformational heterogeneity observed in the protein target.

This work provided a new description of the possible structure of unbound, though catalytically active, WNV NS2B-NS3pro in solution. Sedimentation velocity and SAXS data clearly showed WNV NS2B-NS3pro was monomeric and monodisperse under the tested solution conditions. Moreover, the frictional ratio calculated from sedimentation velocity measurements and pair distance distribution plots suggested the solution structure had a nonglobular elongated shape. Significantly, theoretical scattering curves from the open and closed NS2B-NS3pro crystallographic structures (or a mixture thereof) did not approximate SAXS data measured for WNV protease in solution. *Ab initio* reconstructions and rigid body modeling generated a WNV NS2B-NS3pro conformation that suggested the protease did not adopt a compact structure in solution.

NS2B-NS3pro ensemble models that contained a NS2B chain structured at the C-terminus and flexible at the N-terminus (i.e., NS2B-NT) were not in agreement with the SAXS experimental data. Extending the flexible region of NS2B to the Asp84-Asp85-Asp86 triad did not significantly improve the agreement between the ensemble model (i.e., NS2B-DDD) and SAXS data. Ensemble model NS2B-CTf had a NS2B chain structured at the C-terminus and flexible at the N-terminus; these features

dx.doi.org/10.1021/bi400782w | *Biochemistry* 2013, 52, 6856−6865

were suggested by previous NMR studies of unbound WNV NS2B-NS3pro.[20,21] Unfortunately, this model did not provide good agreement with the SAXS data. The poor fitting between the NS2B-CTf model and the SAXS data suggested that the NMR structure was not a good representation of the conformation the WNV protease adopted in solution under our solution conditions. It is possible the NMR structure of the unbound protease did not serve as a good model for the SAXS data because the severe signal overlap and cross-peak broadening observed in NMR data made initial resonance assignments difficult,[20,21] such that the resonance assignments for the unbound protease were extrapolated from resonance assignments for the ^{15}N HSQC spectra of the protease bound to inhibitor. This extrapolation may have biased the assignments and produced a result where the most populated conformation of the unbound WNV protease was similar to the structure of the protease bound to an inhibitor (i.e., a closed structure). In contrast, the SAXS data collection and subsequent analysis of the unbound protease structure did not rely on data from the protease bound to an inhibitor. As a consequence, the two techniques (SAXS and NMR) could produce different conformations for the protease in solution.

Ensemble models that allowed the N-terminal region of NS2B to be fully mobile with either the C-terminal portion of NS2B (e.g., model NSNS2B-CT) or the linker between NS2B and NS3pro (e.g., NS2B-F) fully flexible agreed very well with SAXS data. Similarly, an ensemble model with a flexible NS2B chain agreed very well with SAXS data. The common feature of these plausible ensemble models was the large degree of flexibility and mobility of the entire NS2B, with no segment of NS2B constrained to the positions shown in the crystallographic structures (Figures 5 and 7). Because it is not possible to "prove" that a model is correct, the NS2B-U and NS2B-F models were used to represent limiting cases in which the NS2B structure was either completely flexible (model NS2B-U) or the conformation of NS2B was fixed but mobile (model NS2B-F). Because both models fit the SAXS data equally well, a plausible interpretation was that the solution state of NS2B existed as a highly mobile extended structure with significant conformational heterogeneity, and that the NS2B could retain some of the secondary structural elements (i.e., β-turns) observed within the NS2B crystallographic structure. Moreover, we cannot exclude the possibility that the solution state of NS2B-NS3pro contained a small part of the NS2B chain (much smaller that the segments constrained in models NS2B-CTf, NS2B-NT, and NS2B-DDD) that was not fully mobile and remained bound to the NS3pro chain; however, our studies have not yet found such a model that would be consistent with the experimental SAXS data. Interestingly, the NS2B-F ensemble may contain two preferred subensembles (Figure 4C), the larger subensemble (85% of the population) being compact ($R_g \sim 22$ Å) and the less populated subensemble being more extended ($R_g \sim 28$ Å). The more populated subensemble could be stabilized by transient interactions between NS2B and NS3pro.

Our FTIR results implied that most (if not all) of the secondary structure observed in the crystallographic structure might be preserved in solution, and that some additional regions (i.e., the highly mobile segments not observed in the crystal structures) of the NS2B-NS3 chains may contain β-structure, perhaps because of transient NS2B-NS3pro interactions. Thus, the NS2B chain, although fully mobile, might retain the secondary structural elements observed in the open and closed crystallographic structures (e.g., the β-hairpin at NS2B residues 78−86). An ensemble of WNV NS2B-NS3pro structures in which much of the NS2B cofactor was flexible but preserved most of the NS2B secondary structure observed by X-ray crystallography might be a good representation of the solution state of NS2B-NS3. We also note that the method used for secondary structure estimation from FTIR spectra can overestimate the β-structure content by as much as 30% relative to crystallographic structures.[40]

With this work, we provided a detailed structural characterization of the solution state of active WNV NS2B-NS3pro, free of mutations and in the absence of substrates or inhibitors that may induce conformational changes in the protein structure. We established that the protease solution state was consistent with a conformational ensemble in which the NS2B cofactor was fully dynamic and likely not bound to the structured NS3pro domain (Figure 7). This insight might contribute to the better rational design of small inhibitors either by restricting the intrinsic flexibility of the protease or by including conformational heterogeneity in ligand binding calculations.

AUTHOR INFORMATION

Corresponding Author

*Department of Biochemistry and Molecular Biology, University of Texas Medical Branch, Galveston, TX 77555. E-mail: watowich@xray.utmb.edu. Telephone: (409) 747-4749.

Funding

This work was supported in part by National Institutes of Health Grant R21 AI066160 and grants from 60° Pharmaceuticals, Inc., and the IBM International Foundation to S.J.W. A.P.G. was supported by the Chilean Government Scholarship, BECA-SCHILE "Programa Formación de Capital Humano Avanzado".

Notes

The authors declare no competing financial interest.

ACKNOWLEDGMENTS

We thank Drs. K. Choi, L. Holthauzen, and C. Soto for assistance with biophysical studies and access to equipment.

ABBREVIATIONS

WNV, West Nile virus; SAXS, small-angle X-ray scattering; R_g, radius of gyration; D_{max}, maximal distance; NMD, normalized spatial discrepancy; FTIR, Fourier transform infrared spectroscopy.

REFERENCES

(1) Mueller, N. H., Yon, C., Ganesh, V. K., and Padmanabhan, R. (2007) Characterization of the West Nile virus protease substrate specificity and inhibitors. *Int. J. Biochem. Cell Biol. 39*, 606−614.

(2) Center of Disease Control and Prevention (http://www.cdc.gov/).

(3) Chappell, K. J., Stoermer, M. J., Fairlie, D. P., and Young, P. R. (2008) West Nile Virus NS2B/NS3 protease as an antiviral target. *Curr. Med. Chem. 15*, 2771−2784.

(4) Shiryaev, S. A., Kozlov, I. A., Ratnikov, B. I., Smith, J. W., Lebl, M., and Strongin, A. Y. (2007) Cleavage preference distinguishes the two-component NS2B-NS3 serine proteinases of Dengue and West Nile viruses. *Biochem. J. 401*, 743−752.

(5) Bera, A. K., Kuhn, R. J., and Smith, J. L. (2007) Functional characterization of cis and trans activity of the Flavivirus NS2B-NS3 protease. *J. Biol. Chem. 282*, 12883−12892.

(6) Falgout, B., Pethel, M., Zhang, Y. M., and Lai, C. J. (1991) Both nonstructural proteins NS2B and NS3 are required for the proteolytic processing of dengue virus nonstructural proteins. *J. Virol. 65*, 2467−2475.

(7) Nall, T. A., Chappell, K. J., Stoermer, M. J., Fang, N. X., Tyndall, J. D., Young, P. R., and Fairlie, D. P. (2004) Enzymatic characterization and homology model of a catalytically active recombinant West Nile virus NS3 protease. *J. Biol. Chem. 279*, 48535−48542.
(8) Chernov, A. V., Shiryaev, S. A., Aleshin, A. E., Ratnikov, B. I., Smith, J. W., Liddington, R. C., and Strongin, A. Y. (2008) The two-component NS2B-NS3 proteinase represses DNA unwinding activity of the West Nile virus NS3 helicase. *J. Biol. Chem. 283*, 17270−17278.
(9) Luo, D., Wei, N., Doan, D. N., Paradkar, P. N., Chong, Y., Davidson, A. D., Kotaka, M., Lescar, J., and Vasudevan, S. G. (2010) Flexibility between the protease and helicase domains of the dengue virus NS3 protein conferred by the linker region and its functional implications. *J. Biol. Chem. 285*, 18817−18827.
(10) Shiryaev, S. A., Ratnikov, B. I., Chekanov, A. V., Sikora, S., Rozanov, D. V., Godzik, A., Wang, J., Smith, J. W., Huang, Z., Lindberg, I., Samuel, M. A., Diamond, M. S., and Strongin, A. Y. (2006) Cleavage targets and the D-arginine-based inhibitors of the West Nile virus NS3 processing proteinase. *Biochem. J. 393*, 503−511.
(11) Knox, J. E., Ma, N. L., Yin, Z., Patel, S. J., Wang, W. L., Chan, W. L., Ranga Rao, K. R., Wang, G., Ngew, X., Patel, V., Beer, D., Lim, S. P., Vasudevan, S. G., and Keller, T. H. (2006) Peptide inhibitors of West Nile NS3 protease: SAR study of tetrapeptide aldehyde inhibitors. *J. Med. Chem. 49*, 6585−6590.
(12) Lim, H. A., Joy, J., Hill, J., and San Brian Chia, C. (2011) Novel agmatine and agmatine-like peptidomimetic inhibitors of the West Nile virus NS2B/NS3 serine protease. *Eur. J. Med. Chem. 46* (7), 3130−3134.
(13) Schuller, A., Yin, Z., Brian Chia, C. S., Doan, D. N., Kim, H. K., Shang, L., Loh, T. P., Hill, J., and Vasudevan, S. G. (2011) Tripeptide inhibitors of dengue and West Nile virus NS2B-NS3 protease. *Antiviral Res. 92*, 96−101.
(14) Ganesh, V. K., Muller, N., Judge, K., Luan, C. H., Padmanabhan, R., and Murthy, K. H. (2005) Identification and characterization of nonsubstrate based inhibitors of the essential dengue and West Nile virus proteases. *Bioorg. Med. Chem. 13*, 257−264.
(15) Johnston, P. A., Phillips, J., Shun, T. Y., Shinde, S., Lazo, J. S., Huryn, D. M., Myers, M. C., Ratnikov, B. I., Smith, J. W., Su, Y., Dahl, R., Cosford, N. D., Shiryaev, S. A., and Strongin, A. Y. (2007) HTS identifies novel and specific uncompetitive inhibitors of the two-component NS2B-NS3 proteinase of West Nile virus. *Assay Drug Dev. Technol. 5*, 737−750.
(16) Mueller, N. H., Pattabiraman, N., Ansarah-Sobrinho, C., Viswanathan, P., Pierson, T. C., and Padmanabhan, R. (2008) Identification and biochemical characterization of small-molecule inhibitors of West Nile virus serine protease by a high-throughput screen. *Antimicrob. Agents Chemother. 52*, 3385−3393.
(17) Ekonomiuk, D., Su, X. C., Ozawa, K., Bodenreider, C., Lim, S. P., Yin, Z., Keller, T. H., Beer, D., Patel, V., Otting, G., Caflisch, A., and Huang, D. (2009) Discovery of a non-peptidic inhibitor of west nile virus NS3 protease by high-throughput docking. *PLoS Neglected Trop. Dis. 3*, e356.
(18) Aleshin, A. E., Shiryaev, S. A., Strongin, A. Y., and Liddington, R. C. (2007) Structural evidence for regulation and specificity of flaviviral proteases and evolution of the Flaviviridae fold. *Protein Sci. 16*, 795−806.
(19) Robin, G., Chappell, K., Stoermer, M. J., Hu, S. H., Young, P. R., Fairlie, D. P., and Martin, J. L. (2009) Structure of West Nile virus NS3 protease: Ligand stabilization of the catalytic conformation. *J. Mol. Biol. 385*, 1568−1577.
(20) Su, X. C., Ozawa, K., Qi, R., Vasudevan, S. G., Lim, S. P., and Otting, G. (2009) NMR analysis of the dynamic exchange of the NS2B cofactor between open and closed conformations of the West Nile virus NS2B-NS3 protease. *PLoS Neglected Trop. Dis. 3*, e561.
(21) Su, X. C., Ozawa, K., Yagi, H., Lim, S. P., Wen, D., Ekonomiuk, D., Huang, D., Keller, T. H., Sonntag, S., Caflisch, A., Vasudevan, S. G., and Otting, G. (2009) NMR study of complexes between low molecular mass inhibitors and the West Nile virus NS2B-NS3 protease. *FEBS J. 276*, 4244−4255.
(22) Schuck, P. (2000) Size-distribution analysis of macromolecules by sedimentation velocity ultracentrifugation and Lamm equation modeling. *Biophys. J. 78*, 1606−1619.
(23) Ortega, A., Amorós, D., and García de la Torre, J. (2011) Prediction of hydrodynamic and other solution properties of rigid proteins from atomic- and residue-level models. *Biophys. J. 17*, 892−898.
(24) Tomlinson, S. M., and Watowich, S. J. (2008) Substrate inhibition kinetic model for West Nile virus NS2B-NS3 protease. *Biochemistry 47*, 11763−11770.
(25) Kuzmic, P. (1996) Program DYNAFIT for the analysis of enzyme kinetic data: Application to HIV proteinase. *Anal. Biochem. 237*, 260−273.
(26) Konarev, P. V., Volkov, V. V., Sokolova, A. V., Koch, M. H. J., and Svergun, D. I. (2003) PRIMUS: A Windows PC-based system for small-angle scattering data analysis. *J. Appl. Crystallogr. 36*, 1277−1282.
(27) Mertens, H. D., and Svergun, D. I. (2010) Structural characterization of proteins and complexes using small-angle X-ray solution scattering. *J. Struct. Biol. 172*, 128−141.
(28) Svergun, D. I. (1992) Determination of the regularization parameter in indirect-transform methods using perceptual criteria. *J. Appl. Crystallogr. 25*, 495−503.
(29) Svergun, D. I., Barberato, C., and Koch, M. H. J. (1995) CRYSOL: A Program to Evaluate X-ray Solution Scattering of Biological Macromolecules from Atomic Coordinates. *J. Appl. Crystallogr. 28*, 768−773.
(30) Franke, D., and Svergun, D. I. (2009) DAMMIF, a program for rapid ab-initio shape determination in small-angle scattering. *J. Appl. Crystallogr. 42*, 342−346.
(31) Volkov, V. V., and Svergun, D. I. (2003) Uniqueness of ab-initio shape determination in small-angle scattering. *J. Appl. Crystallogr. 36*, 860−864.
(32) Bernado, P., Mylonas, E., Petoukhov, M. V., Blackledge, M., and Svergun, D. I. (2007) Structural Characterization of Flexible Proteins Using Small-Angle X-ray Scattering. *J. Am. Chem. Soc. 129*, 5656−5664.
(33) Ken'ichi, A. (2002) Development and Application of Secondary Structural Estimation Program of Protein for FTIR (IR-SSE). *Jasco Rep. 44*, 54−57.
(34) Chappell, K. J., Stoermer, M. J., Fairlie, D. P., and Young, P. R. (2007) Generation and characterization of proteolytically active and highly stable truncated and full-length recombinant West Nile virus NS3. *Protein Expression Purif. 53*, 87−96.
(35) Dam, J., and Schuck, P. (2004) Calculating sedimentation coefficient distributions by direct modeling of sedimentation velocity concentration profiles. *Methods Enzymol. 384*, 185−212.
(36) Celej, M. S., Montich, G. G., and Fidelio, G. D. (2003) Protein stability induced by ligand binding correlates with changes in protein flexibility. *Protein Sci. 12*, 1496−1506.
(37) Manning, M. C. (2005) Use of infrared spectroscopy to monitor protein structure and stability. *Expert Rev. Proteomics 2*, 731−743.
(38) Byler, D. M., and Susi, H. (1986) Examination of the secondary structure of proteins by deconvolved FTIR spectra. *Biopolymers 25*, 469−487.
(39) Haris, P. I., Lee, D. C., and Chapman, D. (1986) A Fourier transform infrared investigation of the structural differences between ribonuclease A and ribonuclease S. *Biochim. Biophys. Acta 874*, 255−265.
(40) Sarver, R. W., and Kruegar, W. C. (1991) Protein secondary structure from Fourier transform infrared spectroscopy: A data base analysis. *Anal. Biochem. 194*, 89−100.
(41) Kong, J., and Yu, S. (2007) Fourier transform infrared spectroscopic analysis of protein secondary structures. *Acta Biochim. Biophys. Sin. 39*, 549−559.